Article

Cell

Plasticity of an Ultrafast Interaction between Nucleoporins and Nuclear Transport Receptors

Graphical Abstract

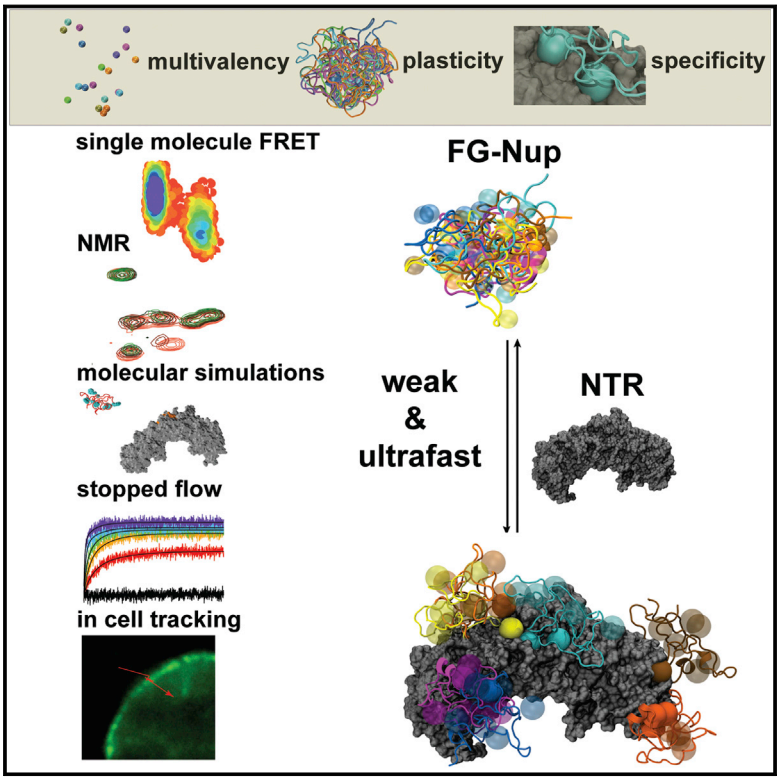

Authors

Sigrid Milles, Davide Mercadante, Iker Valle Aramburu, ..., Martin Blackledge, Frauke Gräter, Edward A. Lemke

Correspondence

martin.blackledge@ibs.fr (M.B.), frauke.graeter@h-its.org (F.G.), lemke@embl.de (E.A.L.)

In Brief

Intrinsically disordered nucleoporins (Nups) engage rapidly with nuclear transport receptors through many minimalistic, weakly binding motifs. These Nups form polyvalent complexes while retaining conformational plasticity thus ensuring both rapid and specific transport.

Highlights

- Integrative structural biology reveals the basis of rapid nuclear transport
- Transient binding of disordered nucleoporins leaves their plasticity unaffected
- Multiple minimalistic low-affinity binding motifs create a polyvalent complex
- A highly reactive and dynamic surface permits an ultrafast binding mechanism

Milles et al., 2015, Cell *163*, 734–745
October 22, 2015
http://dx.doi.org/10.1016/j.cell.2015.09.047

CellPress

Cell

Article

Plasticity of an Ultrafast Interaction between Nucleoporins and Nuclear Transport Receptors

Sigrid Milles,[1,4,5,6,8] Davide Mercadante,[2,3,8] Iker Valle Aramburu,[1,8] Malene Ringkjøbing Jensen,[4,5,6] Niccolò Banterle,[1] Christine Koehler,[1] Swati Tyagi,[1] Jane Clarke,[7] Sarah L. Shammas,[7] Martin Blackledge,[4,5,6,*] Frauke Gräter,[2,3,*] and Edward A. Lemke[1,*]

[1]Structural and Computational Biology Unit, Cell Biology and Biophysics Unit, European Molecular Biology Laboratory (EMBL), Meyerhofstrasse 1, 69117 Heidelberg, Germany
[2]Molecular Biomechanics group, HITS gGmbH, Schloß-Wolfsbrunnenweg 35, 69118 Heidelberg, Germany
[3]IWR – Interdisciplinary Center for Scientific Computing, Im Neuenheimer Feld 368, 69120, Heidelberg, Germany
[4]University Grenoble Alpes, IBS, F-38044 Grenoble, France
[5]CNRS, IBS, F-38044 Grenoble, France
[6]CEA, IBS, F-38044 Grenoble, France
[7]Department of Chemistry, University of Cambridge, Cambridge CB2 1EW, UK
[8]Co-first author
*Correspondence: martin.blackledge@ibs.fr (M.B.), frauke.graeter@h-its.org (F.G.), lemke@embl.de (E.A.L.)
http://dx.doi.org/10.1016/j.cell.2015.09.047

SUMMARY

The mechanisms by which intrinsically disordered proteins engage in rapid and highly selective binding is a subject of considerable interest and represents a central paradigm to nuclear pore complex (NPC) function, where nuclear transport receptors (NTRs) move through the NPC by binding disordered phenylalanine-glycine-rich nucleoporins (FG-Nups). Combining single-molecule fluorescence, molecular simulations, and nuclear magnetic resonance, we show that a rapidly fluctuating FG-Nup populates an ensemble of conformations that are prone to bind NTRs with near diffusion-limited on rates, as shown by stopped-flow kinetic measurements. This is achieved using multiple, minimalistic, low-affinity binding motifs that are in rapid exchange when engaging with the NTR, allowing the FG-Nup to maintain an unexpectedly high plasticity in its bound state. We propose that these exceptional physical characteristics enable a rapid and specific transport mechanism in the physiological context, a notion supported by single molecule in-cell assays on intact NPCs.

INTRODUCTION

The plasticity of intrinsically disordered proteins (IDPs) is thought to be key to their highly diverse roles in the eukaryotic interactome and a variety of vital processes such as transcription, epigenetic regulation mechanisms, and transport through nuclear pore complexes (NPCs) (Dyson and Wright, 2005; Tompa and Fuxreiter, 2008). The central channel of the NPC is filled with phenylalanine-glycine-rich proteins, called FG-nucleoporins (FG-Nups) that are intrinsically disordered (Denning et al., 2003). FG-Nups build up an approximately 30-nm-thick permeability barrier through which large molecules (>40 kDa) can only be shuttled when bound to a nuclear transport receptor (NTR) with passage times as fast as 5 ms (Hoelz et al., 2011; Kubitscheck et al., 2005; Tu et al., 2013; Wälde and Kehlenbach, 2010). Due to the intrinsic dynamics of the FG-Nups, even state-of-the-art electron tomographic studies are not able to visualize them within the central NPC channel, despite their millimolar concentrations (Bui et al., 2013). Consequently, the molecular structure of the permeability barrier and its general mode of action are widely debated (for a review see Adams and Wente, 2013).

The key to understanding the observed nucleocytoplasmic transport phenomena resides in a description of the binding mode between FG-Nups and NTRs, for which a molecular analysis of the FG-Nup•NTR interaction is a prerequisite. Our current understanding of the molecular basis of FG-Nup•NTR interactions is in large part derived from X-ray crystallographic structures or molecular dynamics (MD) simulations of NTRs in the presence of short FG-peptides (up to ~13 amino acids in length) (Bayliss et al., 2000; Isgro and Schulten, 2005), as well as binding measurements with different NTRs or mutated NTR binding pockets (Bednenko et al., 2003; Milles and Lemke, 2014; Otsuka et al., 2008). Even for FG-Nups alone, only overall chain dimensions or long-range interactions within the Nups have so far been analyzed in solution (Milles and Lemke, 2011; Yamada et al., 2010). Notably, even such fundamental binding characteristics as the equilibrium dissociation constant (K_d) between Nups and NTRs are still matter of discussion - estimates range from a few nM to several mM (Bednenko et al., 2003; Ben-Efraim and Gerace, 2001; Tetenbaum-Novatt et al., 2012; Tu et al., 2013). However, high K_d (low affinity, ~mM) values are not easily compatible with high specificity of the transport process, while low K_d values (~nM range) cannot easily explain high transport rates, since these might be expected to correlate with long

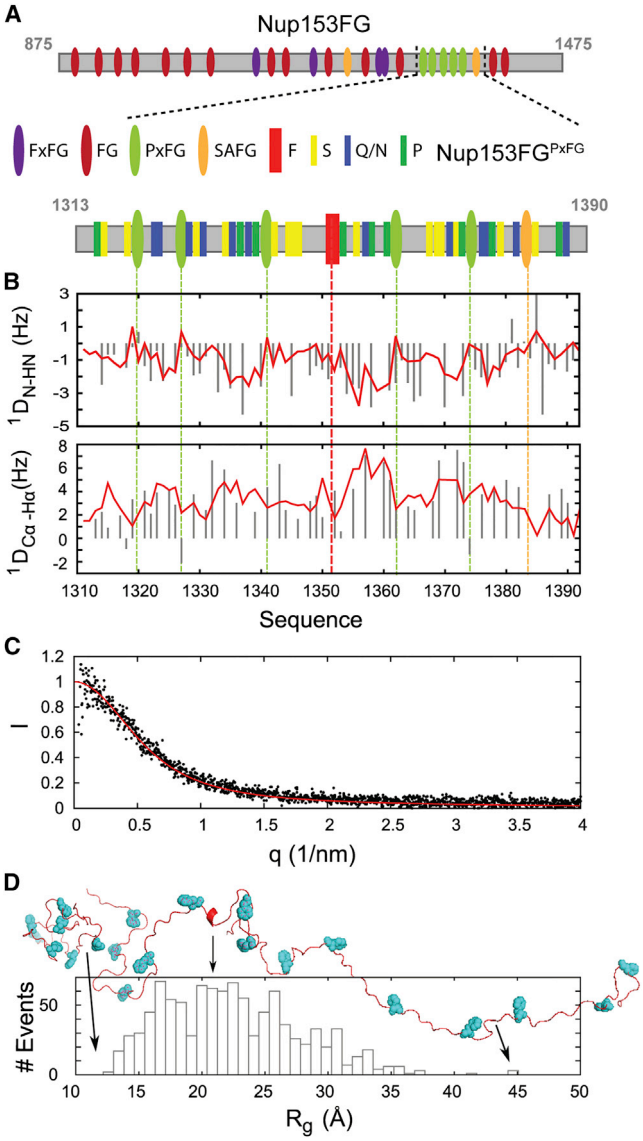

Figure 1. Conformation of Nup153FG^{PxFG}

(A) Scheme of Nup153FG constructs.

(B) Residual dipolar couplings (RDCs) of Nup153FG^{PxFG} aligned in phages. Experimentally obtained RDCs (gray bars) were compared with RDCs calculated from the ASTEROIDS ensemble obtained on the basis of experimental chemical shifts (red line). Dashed lines represent positions of FG-repeats and F1374. Color code as in (A).

(C) The same conformational ensemble was used to calculate a small angle X-ray scattering (SAXS) curve using CRYSOL (red line). The back calculated scattering curve is in good agreement with measured SAXS data under similar experimental conditions (black dots) (Mercadante et al., 2015).

(D) Distribution of the radius of gyration (R_G) from five equivalent ASTEROIDS selections. The three conformations displayed on top represent the most compact, the least compact, and one of the most prevalent conformations in the ensemble.

residence times whereas NTRs must encounter many FG-Nups while crossing the thick barrier.

Fast protein binding also typically requires proper orientation of the protein binding partners as well as conformational adaptation of the IDP to bind to a folded protein. Those can occur prior to or during binding, as described by either of the two prevalent models for protein binding namely conformational selection and induced fit (Csermely et al., 2010; Wright and Dyson, 2009). While such a conformational shift or fit can present the rate-limiting step of binding, fast binding is warranted in many biological processes. Several binding rate enhancing effects have been suggested or observed experimentally, such as maintenance of a degree of disorder (termed ''fuzziness''; Tompa and Fuxreiter, 2008) by conformational funneling (Schneider et al., 2015), a large capture radius of the flexible IDPs (Shoemaker et al., 2000), and the involvement of long-range electrostatic interactions to steer (attract) proteins together (Ganguly et al., 2013).

In this work, we characterize the conformational plasticity of Nups from human and yeast in the presence of structurally and functionally diverse NTRs. A focus was a PxFG-rich domain of the Nup153 (Nup153FG^{PxFG}) as its size permitted a combination of nuclear magnetic resonance (NMR), single molecule Förster resonance energy transfer (smFRET), and molecular dynamics (MD) simulations to characterize local, residue specific, as well as long-range implications of Importinβ binding to Nup153FG^{PxFG} conformation and dynamics. Additional Brownian dynamics (BD), fluorescence stopped-flow and single molecule transport experiments with functional NPCs in permeabilized cells, revealed the detailed kinetics of the complex formation between Nup and NTR. Using this molecular, integrative structural biology approach we propose a mechanism whereby Nups contribute low-affinity minimalistic binding motifs that act in concert to create a polyvalent complex. The global Nup structure and dynamics are largely unaffected by the interaction, thereby ensuring ultrafast binding and unbinding of individual motifs—a result that explains how nuclear transport can be fast yet specific, and that may have general implications for the mechanism of action of other IDPs that exhibit a multiplicity of binding motifs.

RESULTS

Nup153FG^{PxFG} Populates a Disordered Ensemble in Solution

We initially characterized the structure and dynamics of Nup153FG^{PxFG} using high resolution NMR (Figure 1A, sequences given in Supplemental Experimental Procedure). Complete assignment of the backbone resonances (Figure S1) allowed us to develop a multi-conformational model of the protein in solution using a combination of Flexible-Meccano (Ozenne et al., 2012) and the genetic algorithm ASTEROIDS (Jensen et al., 2010). Representative ensembles comprising 200 conformers were selected on the basis of the experimental chemical shifts and were in excellent agreement with $^1D_{N-NH}$ and $^1D_{C\alpha-H\alpha}$ residual dipolar couplings and small angle X-ray scattering (SAXS) curves (Mercadante et al., 2015) that were not used in the selection process (Figures 1B–1D). The amino acid specific backbone dihedral angle distributions determined from the ensemble selections (Figure S1) show that negligible secondary structure is present.

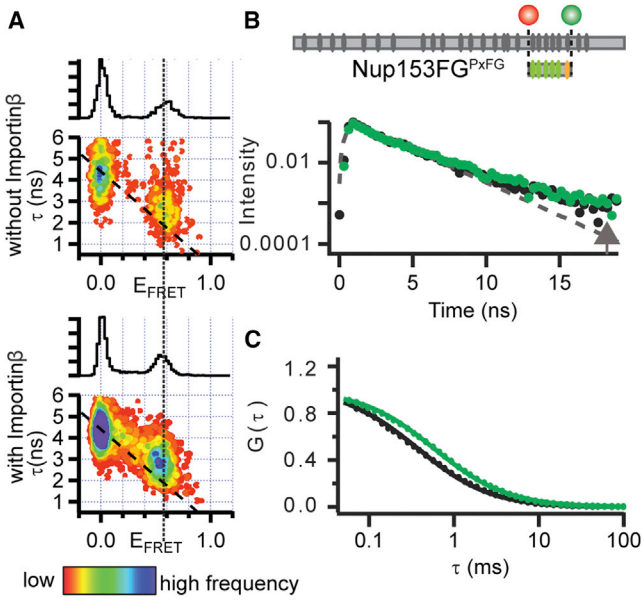

Figure 2. Nup153FG^{PxFG}·Importinβ Interaction Analyzed by smFRET

(A) FRET efficiency (E_{FRET}) versus fluorescence lifetime (τ) histograms of Nup153FG^{PxFG} in the presence and absence of Importinβ. The dotted line visualizes the center position of the FRET peak. The dashed (diagonal) lines show the static E_{FRET} relationship, on which a distribution would lie in the absence of fast dynamics.

(B) Fluorescence lifetimes (τ) of the double labeled population accumulated from single molecule data in the absence (black) and presence (green) of Importinβ. Offset from a single exponential lifetime (dashed gray curve and arrow) is a strong indicator of protein dynamics.

(C) Fluorescence correlation spectroscopy (FCS) traces retrieved from measurements of Nup153FG^{PxFG} (black dots) reflect a slower translational motion in the presence of Importinβ (green dots).

Global Structure and Dynamics of the Nup153FG^{PxFG} Are Retained upon Interaction with Importinβ as Measured by smFRET

We labeled Nup153FG^{PxFG} with a donor (Alexa488) and acceptor dye (Alexa594) for FRET at its C- and N terminus, respectively. This allowed us to measure average distance between the dyes as well as the dynamic properties of the protein using histograms relating FRET efficiency (E_{FRET}) and donor lifetimes (τ) of single molecules (sm), a method widely used to detect even minute changes in structure and dynamics, for example when IDPs bind, fold or expand (Kalinin et al., 2010; Milles and Lemke, 2011; Schuler and Eaton, 2008).

We added unlabeled Importinβ to the FRET labeled Nup153FG^{PxFG} and followed the smFRET response. While the diffusion of Nup153FG^{PxFG} in the absence and presence of Importinβ confirmed the binding of Importinβ under single molecule conditions (Figures 2 and S2), we detected neither substantial changes in E_{FRET} nor in the width of the histograms indicating absence of significant changes in the distance distribution (Figure S2 shows an all F to all A negative control). Indeed, the E_{FRET} populations of the unbound and bound Nup153FG^{PxFG} also overlay very closely with respect to τ, which indicates similarly fast dynamics of both forms (Figures 2 and S2 for detailed analysis of structure and dynamics) (Kalinin et al., 2010).

As smFRET is compatible with large proteins, we were able to repeat the same experiments for the same PxFG region within the full-length Nup153FG (601 amino acids), finding similar characteristics, and suggesting that our truncated Nup153FG^{PxFG} largely retains the conformational sampling from within the whole Nup153FG (Figure S2).

In order to determine the general nature of this binding mode, we repeated the experiments with two different FxFG-rich regions of Nup153FG, as well as the GLFG-rich yeast Nup49 and several different NTRs: i) transportin 1 (TRN1), a transport receptor involved in the import of proteins containing an M9 recognition sequence, ii) nuclear transport factor 2 (NTF2), the import receptor of RanGDP and iii) chromosomal region maintenance 1 (CRM1), a major exportin. While TRN1 and CRM1 have a similar molecular weight and superhelical structure as Importinβ, NTF2 is a much smaller, β sheet-rich dimer (Cook et al., 2007; Morrison et al., 2003). As detailed in Figure S3, despite the very distinct functionalities of the different NTRs, the smFRET and FCS measurements of the different Nups and NTRs indicate similar binding characteristics as for the Nup153FG·Importinβ complex.

Interaction with Importinβ Influences Nup153FG^{PxFG} Only Locally and Transiently

To characterize the effects of Importinβ binding on Nup153FG^{PxFG} at atomic resolution, we titrated Importinβ into a solution of ^{15}N labeled Nup153FG^{PxFG} and measured ^{1}H-^{15}N HSQC spectra at different molar ratios. Peak intensities, as well as $^{1}H^{N}$ and ^{15}N chemical shifts of Nup153FG^{PxFG}, were analyzed for each titration step (Figures 3 and S4). Resonance line broadening, associated with small changes in both $^{1}H^{N}$ and ^{15}N chemical shifts, was observed around all F's in the Nup sequence (Figure 3A). Binding was clearly highly localized, and limited to F's, with only F and the immediately adjacent amino acids being affected by the interaction. Interestingly, one single F, which is not associated with a G, is also involved in binding to Importinβ, showing the largest chemical shift changes in the ^{1}H-^{15}N HSQC spectrum during titration with Importinβ (Figure 3A and S4). ^{15}N relaxation rates measured as a function of molar ratio of Importinβ suggest that, overall, the molecule remains flexible in the complex with the transverse relaxation (R_2) increasing significantly upon Importinβ titration only around the interaction sites (Figures 3C and S4), in agreement with the above smFRET-based observations that global disorder and flexibility are not affected by Importinβ binding. Carr-Purcell-Meiboom-Gill (CPMG) relaxation dispersion experiments (Figure S4) suggested that fast exchange (< 10 μs) between the bound and unbound form of Nup153FG^{PxFG} gives rise to the increased R_2 rates around the interaction sites, which makes it possible to estimate a residue-specific $K_{d,individual}$ for each position in Nup153FG^{PxFG} with Importinβ (Figures 3E, 3F and S4) from the population weighted R_2 measurements. Interestingly, the FG-specific affinities to Importinβ are not identical across the Nup153FG^{PxFG} sequence, implying a contribution of inter-FG residues to binding, although all FG-specific $K_{d,individual}$ values lie in the millimolar range.

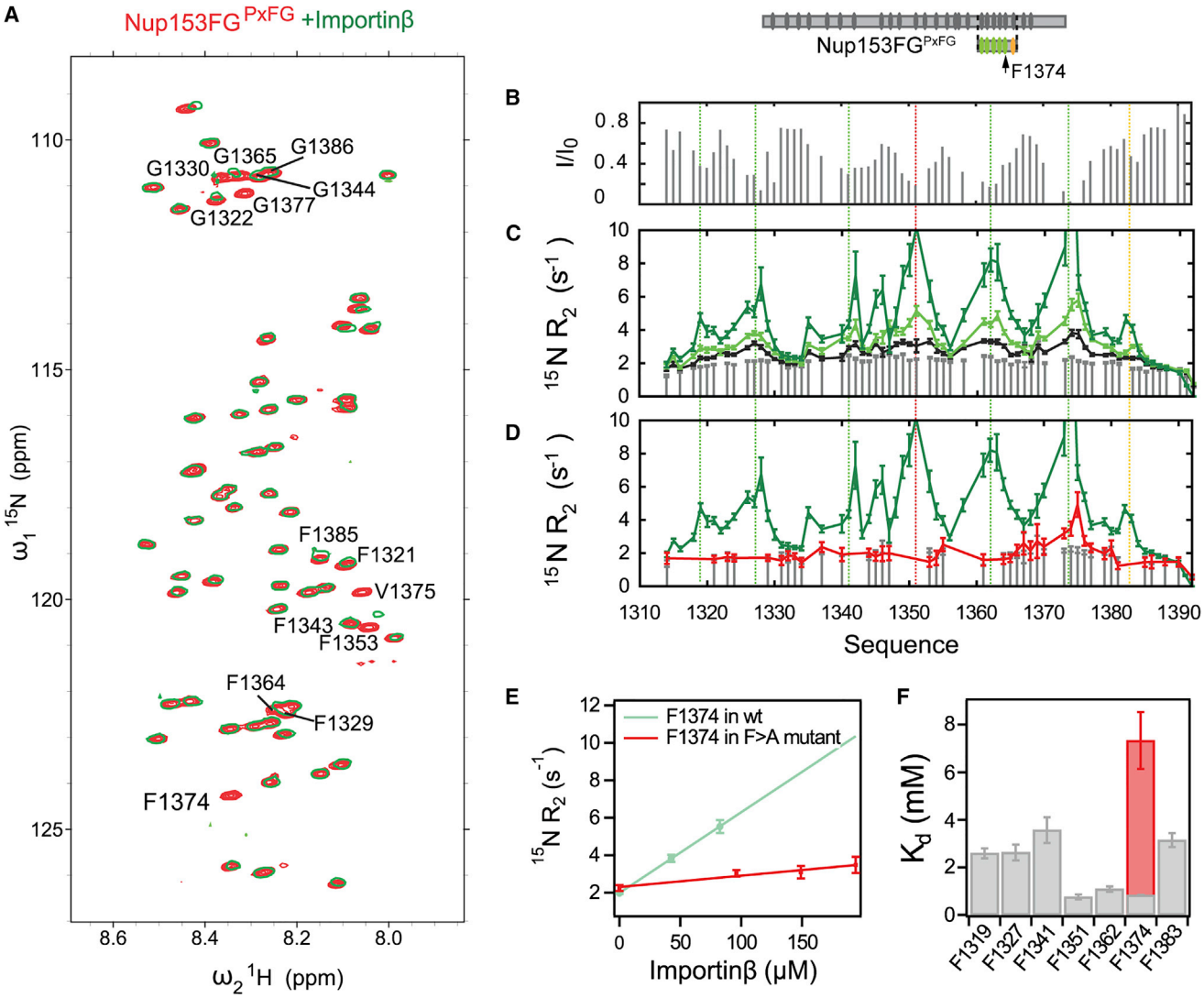

Figure 3. Nup153FG^{PxFG}·Importinβ Interaction by NMR Spectroscopy

(A) ^{1}H-^{15}N HSQC spectrum of Nup153FG^{PxFG} (red) overlayed with a spectrum of Nup153FG^{PxFG} in the presence of Importinβ (green, Nup to NTR molar ratio of 1.14, at a Nup concentration of 240 μM).

(B) The intensity ratio of the bound and unbound form of Nup153FG^{PxFG} was plotted under the same conditions as in (A).

(C) ^{15}N R_2 relaxation rates at 25°C and a ^{1}H frequency of 600 MHz were measured at different concentrations of Importinβ (gray bars are without Importinβ; black, light green and dark green at Importinβ/Nup153FG^{PxFG} molar ratios of 0.17, 0.33, and 0.72 at the constant Nup153FG^{PxFG} concentration of 250 μM).

(D) ^{15}N R_2 of Nup153AG$^{PxAG,\ F1374}$ in the absence (gray) and in the presence of Importinβ (red) overlayed with the rates for Nup153FG^{PxFG} in the presence of Importinβ under the same conditions (green).

(E) For all F in the Nup153FG^{PxFG} sequence, ^{15}N R_2 values were plotted against Importinβ concentration and fitted with a linear slope. The same analysis was performed for F1374 in Nup153AG$^{PxAG,\ F1374}$ and compared to the same F in Nup153FG^{PxFG} (compare red to green slope). R2 with errors greater than 20% were excluded from the analysis.

(F) Local K_d values were calculated from the slopes obtained in Figure S4. Gray bars correspond to K_d values obtained from Nup153FG^{PxFG}, the red bar shows the local K_d of Nup153AG$^{PxAG,\ F1374}$ binding to Importinβ.

Error bars show SD.

Strikingly, when studying the binding to different NTRs like TRN1 and NTF2 (Figure S4), despite exhibiting different binding preferences for FG-Nups (Cook et al., 2007; Milles and Lemke, 2014), their binding modes are remarkably similar to that of the Importinβ complex. The same regions in Nup153FG^{PxFG} are affected by the interaction, again with very low residue specific affinities, with the Nup remaining overall flexible when bound while interacting only locally as seen from both chemical shift changes, in the case of NTF2, and remarkably similar locally elevated transverse relaxation rates in TRN1 (Figure S4). Comparison of ^{13}C backbone chemical shifts measured in the free and NTF2-bound forms of Nup153FG^{PxFG} demonstrates that

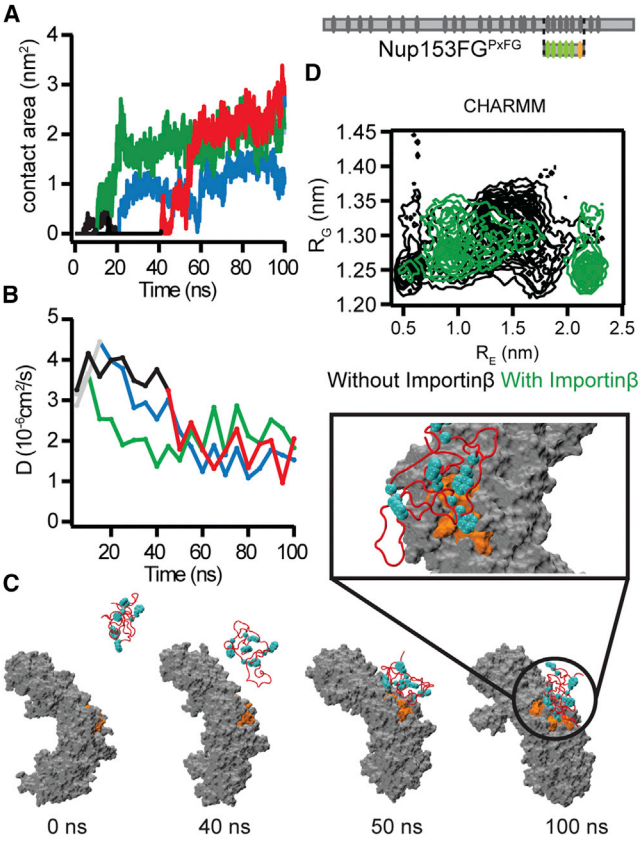

Figure 4. Binding of Nup153FG^{PxFG} to Importinβ^{N}

(A–C) Contact area between (A) Nup153FG^{PxFG} and Importinβ^{N} and (B) diffusion coefficients D as a function of time for the 4 binding events out of 10 simulations (gray/black: prior to binding; different colors: after binding; black/red curves refer to the cartoon in (C) sampled using CHARMM22* force field. (C) Snapshots collected along one of the recorded MD trajectories showing the binding between Nup153FG^{PxFG} (red cartoon) and Importinβ^{N} (gray surface). The binding sites on Importinβ^{N} and Nup153FG^{PxFG} FG-repeats are colored in orange and cyan respectively.

(D) Nup153FG^{PxFG} radius of gyration (R_G) as a function of end-to-end distance (R_E) for the unbound (black) and bound (green) ensembles of Nup153FG^{PxFG} obtained from the simulations performed using CHARMM22*.

See Figure S5 for data using the AMBER force field.

the protein backbone remains flexible upon interaction, sampling effectively the same conformational equilibrium in the free and bound state (Figure S4).

We note that during the publication process of this work, localized interaction was also reported for the yeast Nsp1 with Kap95 (the yeast homolog of Importinβ) using NMR (Hough et al., 2015), suggesting that a similar interaction mechanism may also be conserved across species.

Co-operativity of FG-Nup·Importinβ Binding

To further quantify the action of multiple FG-repeats, we designed a Nup construct, in which all F of Nup153FG^{PxFG} except F1374, the strongest interaction site for Importinβ, were replaced by A (Figure S1). Titration of Importinβ into this Nup153AG^{PxAG,F1374} mutant resulted in strongly reduced peak broadening and negligible chemical shift changes compared to Nup153FG^{PxFG} (Figure S4). As in the case of Nup153FG^{PxFG}, ^{15}N R_2 relaxation rates of Nup153AG^{PxAG,F1374} at the interaction site exhibited a linear dependence on Importinβ concentration (Figure 3E). However the effective $K_{d,individual}$ from F1374 within Nup153AG^{PxAG,F1374} reveals significantly weaker binding for this interaction site than for F1374 when situated within the wild-type (WT) protein ($K_{d,individual}$ = 7.3 mM compared to 0.8 mM, Figure 3). This result clearly shows that presenting multiple equivalent binding sites to the binding partner has a measurably positive effect on the effective affinity of the individual interaction site.

Monitoring the Nup153FG^{PxFG}·Importinβ Binding Using All-Atom MD

We employed MD simulations to investigate the experimental observations of Nup153FG^{PxFG}·Importinβ association from NMR and smFRET. From a broad ensemble of Nup153FG^{PxFG} obtained from unbiased MD simulations in explicit solvent (Movie S1), we incubated different conformers with the N-terminal portion of Importinβ (from here named Importinβ^{N} (Bayliss et al., 2000)) and monitored their binding for a total simulation time of 2 μs (Figures S5 and S6, and Table S1). The association of Nup153FG^{PxFG} to Importinβ^{N} was repeatedly observed within the simulated timescale and occurred in a specific manner (Figures 4 and S5, and Movie S2). FG-repeats docked into previously identified binding pockets on the surface of Importinβ^{N} and even formed contacts similar to those previously observed crystallographically upon interaction between Importinβ and Nsp1-derived peptides (Figures 4C and S6) (Bayliss et al., 2000). Binding was reduced and less specific for Nup153FG^{PxAG} (Figure S5), in agreement with NMR and smFRET (Figures S1, S2, and S4).

We suggest that the high solvent exposure of Fs in the unbound state (typically contained within the hydrophobic interior of folded proteins) (Figure S5) renders them readily available for Nup153FG^{PxFG}·Importinβ^{N} association, without requiring any global structural transitions in either partner (Figures 4D, S6, Movie S2).

The ability to monitor spontaneous Nup153FG^{PxFG}·Importinβ^{N} association on the sub-microsecond timescale suggests an ultrafast association (Figure S5). Underlining the generality of our observation, we were also able to monitor such a spontaneous binding event when repeating simulations for an FxFG-rich region of Nup153 binding to Importinβ^{N} (Figure S5, Movie S3, sequences given in Supplemental Experimental Procedure). However, force field inaccuracies and limited sampling prohibit the reliable extraction of an association rate, and we therefore studied the interaction further through fluorescence stopped-flow experiments (FSF) and Brownian dynamics (BD) simulations.

FSF Experiments and BD Simulations Reveal Ultrafast Binding between Nup and Importinβ

Stopped-flow kinetics monitoring fluorescence anisotropy (*r*) can be used to study binding mechanisms and measure the association rate (k_{on}) between proteins (Shammas et al., 2013). The binding of Importinβ to Nup153FG site-specifically labeled with Cy3B elicits detectable changes in *r*, due to slowed rotational

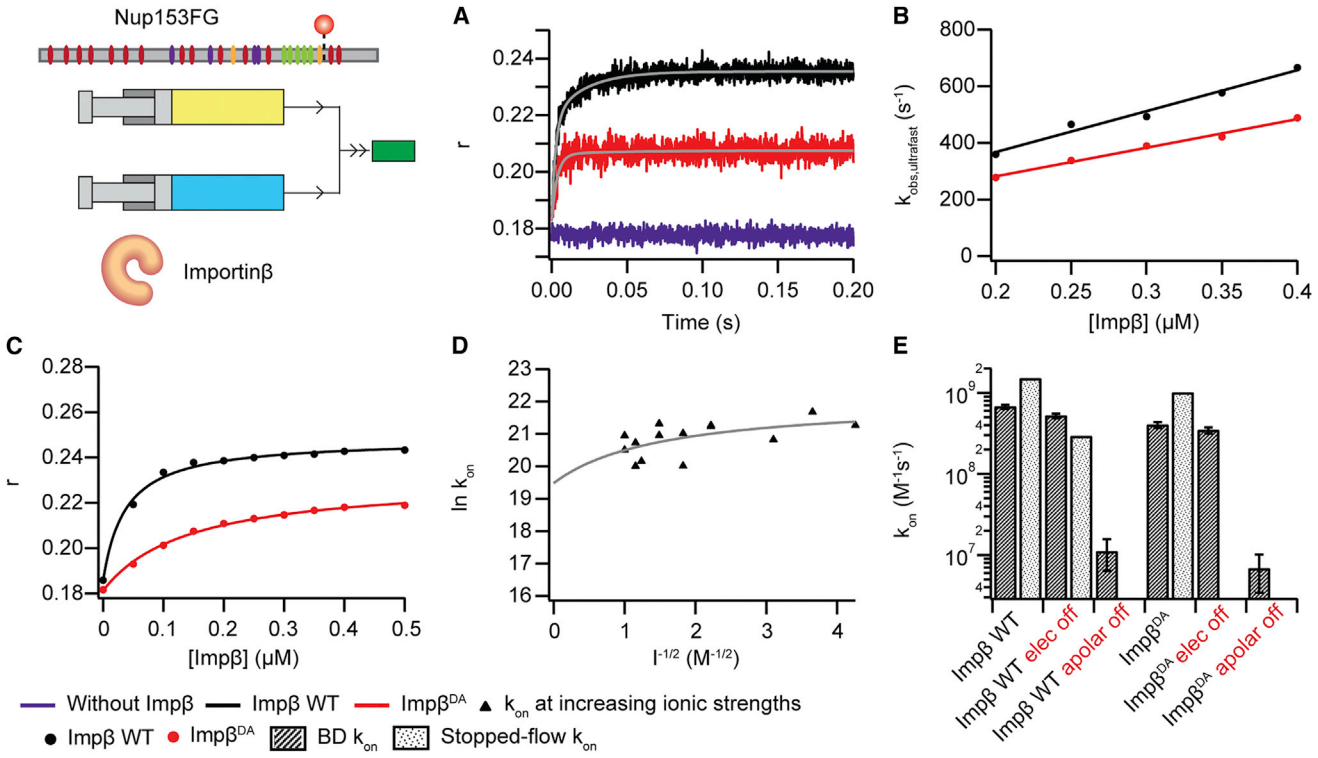

Figure 5. Association Kinetics for Nup153FG with Importinβ

(A) Stopped-flow fluorescence anisotropy was used to monitor the binding of Importinβ (Impβ) at different concentrations to Nup153FG-Cy3B. A selection of anisotropy (r) traces against time is shown for Nup153FG alone (purple) and for the binding of Importinβ WT (black) and Importinβ^{DA} (red).

(B) The observed rates ($k_{obs,ultrafast}$) from association experiments were plotted against the different Importinβ concentrations, the data were linearly fitted to obtain the association rate constants ($k_{on,ultrafast}$).

(C) Apparent $K_{d,app}$ values under the different experimental conditions.

(D) k_{on} obtained from association experiments of Nup153FG and Importinβ at different ionic strengths fitted with a Debye-Hückel-like approximation to calculate the basal rate constant at infinite ionic strength.

(E) Summary of the k_{on} values obtained from BD (dark bars) and FSF measurements (light bars) (Table S2D).

Error bars show SD.

motion (Milles and Lemke, 2014). Since Nup153FG^{PxFG} has only a very small overall binding affinity toward Importinβ, we could not detect a sufficiently strong signal change in the anisotropy measurements in the tested and experimentally feasible concentration range (Figure S7). Thus, for FSF, we used fluorescently labeled full-length Nup153FG. We performed rapid mixing experiments under pseudo-first order conditions in "physiological" transport buffer. A monoexponential function does not describe well the observed anisotropy changes in Figure 5 (Figure S7 and Table S2). This is likely a result of having multiple different binding motifs and/or the ability of multiple Importinβ to engage into binding a single Nup, which adds another level of complexity (multivalency) (Milles and Lemke, 2014; Schoch et al., 2012; Wagner et al., 2015). A biexponential equation is able to describe the kinetics, resulting in two k_{obs} per Importinβ concentration (Figures 5A, 5B, and S7). The fluorescence anisotropy at the end of the reaction was used to calculate the apparent $K_{d,app}$ (Figure 5C). Remarkably, by performing experiments at multiple NTR concentrations we extracted an ultrafast $k_{on,ultrafast}$ = $1.5 \cdot 10^9$ $M^{-1}s^{-1}$ (Figure 5B) for the major component (average amplitude of 70%), while the second component was still very fast, with a $k_{on,fast}$ = $6.1 \cdot 10^7$ $M^{-1}s^{-1}$ at room temperature. These FSF measurements report on overall formation of the Nup153FG• Importinβ complex i.e., one or more F binding. While we provide all results and further analysis details in Figure S7 and Table S2, for later discussion we focus on the fastest measured $k_{on,ultrafast}$.

We next estimated association rates from BD simulations, which compared to MD permit larger statistical sampling, at the cost of freezing the internal dynamics of the binding partners. Upon successful complex formation, starting from the conformations obtained from MD, the association rate was estimated (Figure S7) to be around 10^9 M^{-1} s^{-1} (Figure 5E), in agreement with stopped-flow measurements.

BD simulations carried out without the contribution of apolar desolvation generated a drastic decrease of the estimated $k_{on,BD}$ by around two orders of magnitude, while the absence of electrostatic interactions had a negligible effect (Figures 5E and S7, and Table S2D and S2E). These observations complement our evidence for an association mainly favored by the energetic gain of sequestrating F residues from the solvent and burying them into the Importinβ^N binding pockets.

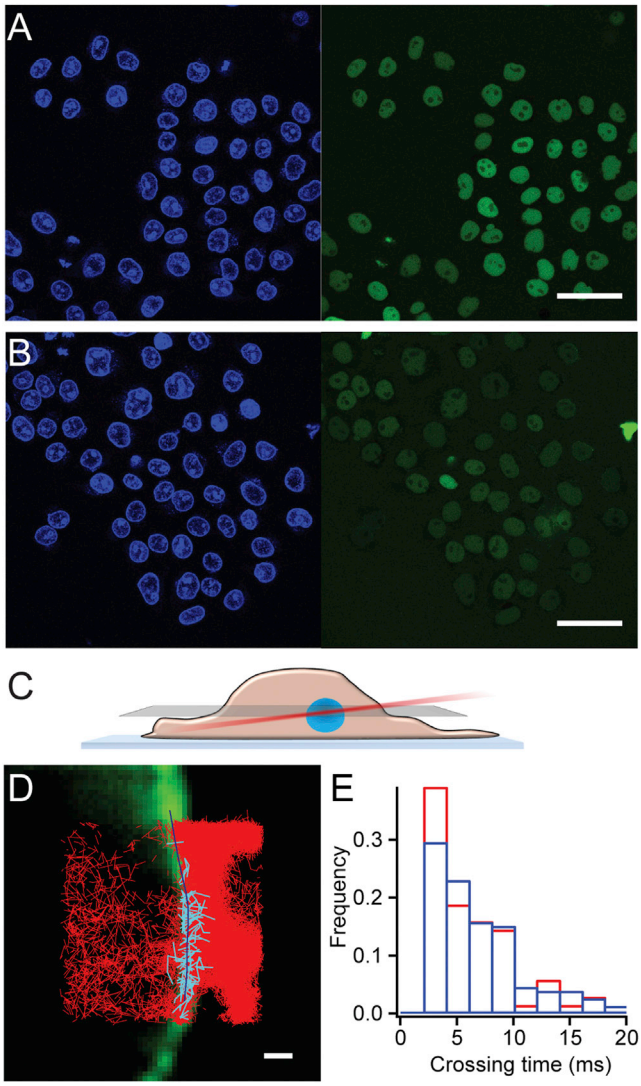

Figure 6. Nuclear Transport Assays of Importinβ and Importinβ^{DA}

(A and B) DAPI staining shown in blue, and green fluorescent cargo (NLS-MBP-eGFP) in permeabilized HeLa cells incubated with either Importinβ (A) or Importinβ^{DA} (B) (scale bar 50 μm). After 45 min, cargo accumulation is higher in the nucleus in (A).

(C) Single molecule trajectories of fluorescently labeled Importinβ were acquired in the equatorial plane of the nucleus exploiting an inclined (Hilo) illumination.

(D) Representative image of acquired single molecule trajectories of Importinβ-Alexa488 (red lines) overlaid with the ensemble image of Importinβ-Alexa647 (in green, scale bar 1 μm) used to identify the nuclear envelope position (blue line). Single particle tracks of the fluorescently labeled NTR (cyan lines) crossing the nuclear envelope were analyzed to yield the characteristic barrier crossing time.

(E) The crossing time distributions reported for Importinβ (blue bars) and Importinβ^{DA} (red bars) are very fast.

While desolvation effects cannot easily be tested experimentally, high ionic strength buffers can be used to shield long-range electrostatic interactions. We thus performed a salt titration ranging from 0.05 to 1 M ionic strength (using NaCl), permitting an estimate of k_{on} under infinite electrostatic shielding by extrapolation using a Debye-Hückel-like approximation (Figures 5D and S7 and Table S2B) (Shammas et al., 2014). In line with the BD simulations, we obtained a $k_{on,elect\ off}$ of $2.9 \cdot 10^8\ M^{-1}s^{-1}$, i.e., binding remains very fast even under electrostatic shielding.

Additional stopped-flow measurements probing different Nup153FG regions (FxFG-, PxFG-rich) with diverse NTRs (NTF2, TRN1, Importinβ) are shown in Figure S7 and Table S2C. In all cases, we observed similar remarkably fast kinetics yielding consistent results for $k_{on} > 5 \cdot 10^8\ M^{-1}s^{-1}$.

Previously, solid phase binding assays indicated that the Importinβ double mutant (I178D/Y255A, termed Importinβ^{DA}) has a more than 60-fold lower K_d for binding to full-length Nup153FG as compared to Importinβ WT (Bednenko et al., 2003). $k_{on,BD}$ dropped by only 40% compared to Importinβ WT, which we confirmed by experimental FSF studies (drop of $k_{on,FSF}$ by 30%, Figure 5). However, fluorescence anisotropy measurements revealed an Importinβ^{DA} titration curve (Figure 5C) that confirms altered binding as compared to Importinβ WT, as e.g., due to an increase in k_{off}.

Single-Particle Tracking Connects Nuclear Transport of Importinβ^{DA} and Importinβ with FG-Nup Association Rates

The efficiency of an NTR to bring cargo across the NPC barrier can be assayed using standard NPC transport assays. In these assays, a fluorescent cargo (NLS-MBP-eGFP) recognized by the Importinβ transport machinery is incubated with permeabilized cells in the presence of a functional transport system and the resulting nuclear fluorescence is measured. In line with the previously reported lower K_d of Importinβ^{DA}, cargo accumulated slower compared to Importinβ WT measurements (Figures 6A and 6B) which can e.g., be due to a lower barrier crossing time, a reduced docking efficiency to the NPC or cargo release from the NPC for example.

A prediction from our kinetic analysis is that the actual speed of barrier crossing, which involves several binding and unbinding steps between NTR and FG repeats should be rather similar for WT and mutant Importinβ, as changes in k_{on} were small, and if at all, a higher k_{off} for the mutant would make crossing even faster (see discussion).

In contrast to the "bulk" transport assay, the speed of barrier crossing (characteristic crossing time) can be measured directly using single molecule (sm) tracking assays (Figure 6C), in which individual Importinβ molecules are fluorescently labeled and tracked while they cross from one side of the NPC to the other. This yielded a typical value of 6.9 ± 0.2 ms for Importinβ and 6.1 ± 0.5 ms for Importinβ^{DA} for barrier crossing (Figures 6D and 6E). We note that this crossing time is near the sampling limit of our technology, and thus faster crossing times cannot easily be captured.

DISCUSSION

The realization that many proteins are disordered has attracted considerable attention to the study of the molecular mechanisms controlling their interactions (Csermely et al., 2010; Tompa and Fuxreiter, 2008; Wright and Dyson, 2009), including the role of disorder in promoting or facilitating binding. In particular, very

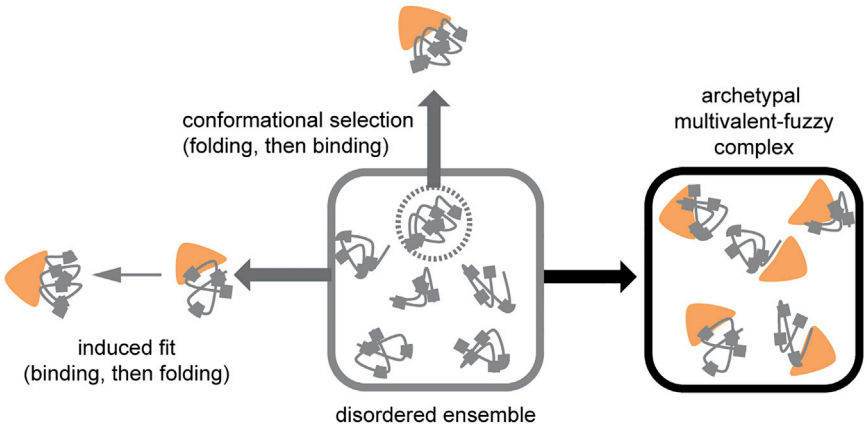

Figure 7. Binding Modes of IDPs to Folded Proteins

Schematic representation of various models describing the binding of an IDP to its folded partner. In an induced-fit mechanism the IDP partially or completely folds upon interacting with its partner, potentially showing an intermediate encounter complex as in the fly-casting mechanism (Shoemaker et al., 2000). In a conformational selection mechanism, the folded protein selects one (or several) conformation(s) of the IDP that best fits its binding pocket. These models suggest a shift in the IDP's conformational ensemble. For the Nup•NTR complex we observed formation of an "archetypal" fuzzy and multivalent complex, a binding mode that on a global scale does not require major energy or time investment for the Nup to transit from its free to the bound conformation. Note that multiple NTRs can bind one Nup and vice versa.

little is known about the binding mechanisms involved in complex processes such as nucleocytoplasmic transport, where NTRs have to engage in multiple, specific binding and unbinding events while traversing a tens of nanometer thick permeability barrier.

In this study, we have used a multidisciplinary approach to investigate the molecular mechanism underlying the interaction process between NTRs and Nups. In general, from our three core findings a coherent view emerges on how multiple rapid, yet specific protein interactions can be achieved.

Nup153FG Forms a Highly Dynamic Complex with Importinβ

Based on our smFRET measurements, we found that Nup153FG^{PxFG} resembles full-length Nup153FG with respect to its dynamics (Figures 2 and S2). Upon interaction with Importinβ, Nup153FG^{PxFG} remains flexible, engaging with Importinβ only locally, as is evident from peak broadening in the respective ^{1}H-^{15}N HSQC spectra as well as R_2 relaxation rates (Figures 3, S1, and S4). Local backbone sampling even of the interacting F was not measurably modified upon interaction. The conformers of Nup153FG^{PxFG} that were subjected to Importinβ^{N} binding in the MD simulations were also devoid of large-scale conformational changes, and interactions were only observed between individual surface exposed residues of Nup153FG^{PxFG} and Importinβ^{N}.

It appears therefore that globally, the FG-Nup maintains its conformational ensemble as shown by smFRET. This observation is sound, as IDPs frequently use motif binding to engage with their binding partners (Kragelj et al., 2015; Schneider et al., 2015; Tompa and Fuxreiter, 2008; Wright and Dyson, 2009). Our observation suggests an extraordinarily small motif (the side chain of F), which would be difficult to identify from large-scale bioinformatics approaches (Dinkel et al., 2014).

The observed binding mode appears distinct from other single motif binding interactions, as well as from mechanisms that involve global conformational transitions, such as folding upon binding (Csermely et al., 2010; Wright and Dyson, 2009) (Figure 7). The intrinsic flexibility of the Nup, the repeated occurrence and short length of the binding motif seem to create a highly reactive binding surface, which renders the individual FG-motifs prone to bind at any time without compromising the Nup's inherent plasticity.

Ultra Rapid Association of the Nup153FG·Importinβ Complex

The maximal association rate in the absence of electrostatic forces for a binary interaction system (in which all collisions are productive) can be approximated by the Einstein-Smoluchowski diffusion limit, which yields a theoretical k_{on} of $\sim 10^9$ $M^{-1}s^{-1}$ for the interaction of proteins of the size of Nup153FG and Importinβ.

Very high association rates have been observed previously in the presence of long-range electrostatic attractions (10^8-10^{10} $M^{-1}s^{-1}$) for example for the barnase/barstar interaction (Spaar et al., 2006), as well as for small IDP complexes studied by NMR (Arai et al., 2012; Schneider et al., 2015). In the absence of electrostatic steering, this upper limit is typically never reached, as successful collisions require proper orientation of the binding partners. Consequently, most experimentally observed association rates at high salt concentrations fall into the regime of 10^4–10^6 $M^{-1}s^{-1}$ (Shammas et al., 2013, 2014).

Our ensemble FSF kinetics (for Nup153FG) and BD simulations (for Nup153FG^{PxFG}) show a k_{on} of $\sim 10^9$ $M^{-1}s^{-1}$ (Figure 5) supporting the aforementioned idea of a strongly reactive binding surface. We specifically observe an influence of apolar desolvation energies in the BD simulation and electrostatics are not found to play a major role in association. This applies apparently to both, Nup153FG^{PxFG}, which is uncharged and was tested in BD, as well as Nup153FG, which has several charges in the N-terminal regions (Figures 5D and S2). Even in the limiting case of electrostatic shielding we found complex formation to still have a remarkably fast $k_{on,FSF}$ (Figures 5D, 5E and Table S2B).

While experimentally bridging the gap between our molecular-level description of the small binary Nup•NTR complex (160 kDa) in solution to the actual in vivo transport mechanisms (involving ~120 MDa NPCs) is still a challenging quest, the sm transport

experiments (Figure 6) underline that the initially unexpected kinetic findings for the Importinβ^{DA} mutant are in line with the finding in functional NPCs.

Individual FG-Repeats Bind with Low Affinity and Act in Concert for Efficient Binding

According to ensemble titration fluorescence curves, we have observed an apparent local equilibrium constant ($K_{d,app}$) between Nup153FG and Importinβ in the nanomolar regime (Figure 5C and Table S2). However, we report millimolar affinities per FG-motif from our NMR measurements within Nup153FG^{PxFG} (Figures 3 and S4), in line with a recent computational model (Tu et al., 2013). Our NMR studies further suggest that individual FG-motifs bind independently of each other, as the ^{15}N R_2 rates are similar to the values of the unbound Nup between the FG-repeats. Nevertheless, the sum of FG-motifs influences the effective binding strength of individual FGs to Importinβ, as can be seen by comparing the effective K_d for F1374 in the WT and the Nup153AG$^{PxAG,\ F1374}$ mutant (Figure 3, S1, and S4).

While these estimates of K_d values (from NMR and ensemble fluorescence) were measured on different Nup constructs, they also report on two different properties: the binding of Importinβ to a larger region of Nup153FG (fluorescence anisotropy) and to a single FG-motif (NMR), and illustrate an important characteristic of the system, namely the importance of polyvalent interactions, which is exploited also by other transport receptors (Figure S4). While an individual FG-motif might be unlikely to be bound, the chances that at least one FG-motif within the Nup molecule is bound may remain high. This stabilizing effect of multivalency/polyvalency is well known, and is even used as a design principle in enhancing the affinity of ligand interactions with multi-site targets where ligands are connected in tandem via short linkers (Brabez et al., 2011; Kramer and Karpen, 1998). Stability enhancements achieved in such experiments can approach four-to-five orders of magnitude and are primarily due to substantial decreases in the global dissociation rate, i.e., in a multivalent system the molecules only separate as a result of a dissociation event if all other motifs are unbound.

To demonstrate generality of these three core findings, we performed additional smFRET, FCS (Figures S2 and S3), NMR (Figure S4), MD (Figure S5 and Movie S3), and FSF experiments (Figure S7 and Table S2C) on a variety of different Nups from human and yeast, including the most common motif in vertebrates (FxFG) and the crucial GLFG sequence in yeast, for a diverse set of NTRs (NTF2, TRN1, CRM1, Importinβ). All results are in close agreement, highlighting the universal nature of the observed mechanism.

Currently, several models are discussed on how a permeability barrier in the NPC can be built; among those are the selective phase, the brush, the reduction of dimensionality and the karyopherin centric model, etc., as well as mixtures of those (Eisele et al., 2013; Frey and Görlich, 2007; Jovanovic-Talisman et al., 2009; Lim et al., 2007; Lowe et al., 2015; Moussavi-Baygi et al., 2011; Peters, 2009; Wagner et al., 2015; Yamada et al., 2010). These models vary mainly over how FG-Nups are arranged and potentially interlinked inside the NPC to create a tight barrier. However, common to all these models is that the concentration of FG-repeats of about 50 mM creates a very crowded environment, which is roughly in line with stoichiometric measurements of Nups and the overall size of the central channel (Bui et al., 2013; Ori et al., 2013). Independently of the transport model assumed, mobility of an NTR inside the barrier is thus largely limited by the k_{off} and k_{on} of the interaction between FG-Nups and NTRs. This is also the case if FGs interact with FGs inside the barrier as proposed in the selective phase model (Frey and Görlich, 2007), as long as these interactions are highly dynamic and do not pose a substantial energetic barrier or rate-limiting step to be melted. That we do not observe obvious FG-FG interactions in our studies is thus not necessarily inconsistent with such a model.

If we were to naively consider the characteristic time for a single Nup and Importinβ to separate based on commonly measured fast k_{on} and affinities (e.g., K_d (Nup•NTR) ~100 nM and k_{on} ~10^6 $M^{-1}s^{-1}$ → unbinding time (UT) ~100 ms), it appears impossible that Importinβ could cross a 50 mM FG-filled pore within 5 ms. This is the previously described "transport paradox," in which high specificity is somehow coupled with rapid transport (Bednenko et al., 2003; Ben-Efraim and Gerace, 2001; Tetenbaum-Novatt et al., 2012; Tu et al., 2013).

Our work (down to picosecond and atomic resolution) is largely compatible with the existing barrier models, as it addresses on a molecular mechanistic level how an NTR could rapidly pass through a dense barrier. Using a simple model of a bivalent system, we already expect an order of magnitude difference between the dissociation rate for an individual motif and that for the whole protein (Kramer and Karpen, 1998). We have also observed extremely rapid association rates (~10^9 $M^{-1}s^{-1}$) and in Supplemental Experimental Procedures (two toy models) we outline that if we consider a very rough estimate for the characteristic time for an individual motif unbinding event (UT~1 μs) for full-length Nup153 (>24 valencies), it becomes clear that the Importinβ could "creep" through the dense FG-motif plug of the pore within the short transport time. Such movement is consistent with our (Figure 6) and other NTR diffusion studies through NPCs in intact cells and various model systems (Eisele et al., 2013; Frey and Görlich, 2007; Jovanovic-Talisman et al., 2009; Moussavi-Baygi et al., 2011; Schleicher et al., 2014; Tu et al., 2013; Wagner et al., 2015).

In this case, nature has achieved a combination of high specificity with fast interaction rates. This is based on many individual low-affinity motifs paired with a binding mode that requires relatively little energy or time investment for the Nup to transit between free and bound conformations, and provides a rationale for the fast, yet specific, nuclear transport. While rapid binding can in principle be realized between proteins of single binding elements (e.g., driven by strong electrostatics), the proofreading emanating from the multiplicity and rapid repetition of many such events is what contributes to specific transport.

We note that the transport paradox goes far beyond the relevance for the transport mechanism, since transient, but targeted interactions are central to the emerging view of highly dynamic protein (and other biomolecular) interaction networks. Furthermore, FG-repeats are also present in stress and P granules (Toretsky and Wright, 2014). It seems likely that such ultrafast binding mechanisms are also important for other biological

recognition processes, where individual interaction motifs only make weak contributions, as e.g., in the recognition of glycans (Ziarek et al., 2013), or other very short linear motifs, like WG motifs in small RNA pathways (Chekulaeva et al., 2010), or binding of proteins to epigenetic marks, like many histone modifications.

In addition, ultrafast association is achieved by using the unique plasticity of multivalent disordered proteins, which is distinct from mechanisms where orientation specific binding is required for complex formation. This represents an additional biological advantage for IDPs in comparison to folded proteins, and might have further facilitated their enrichment in organisms of higher complexity.

EXPERIMENTAL PROCEDURES

Expression and Purification of Importinβ, TRN1, NTF2, CRM1 and Nup153FG

The proteins were purified essentially as described in (Milles and Lemke, 2014) following routine column chromatography and then transferred into the respective measurement buffers. Labelling of Nup153FG (amino acids 875 to 1475 of the full length Nup153; numbering with respect to the full length protein as in 'UniProt: P49790') was performed using routine procedures to introduce Alexa488 as a donor and Alexa594 as an acceptor dye for smFRET experiments (and analog for other dyes), as described in (Milles and Lemke, 2011)

NMR Studies of Nup153FG^{PxFG}

Spectral assignments of ^{13}C, ^{15}N Nup153FG^{PxFG} were obtained from a set of BEST-TROSY-type triple resonance spectra: HNCO, intra-residue HN(CA)CO, HN(CO)CA, intra-residue HNCA, HN(COCA)CB, and intra-residue HN(CA)CB (Solyom et al., 2013). For the measurements of RDCs, ^{13}C, ^{15}N Nup153FG^{PxFG} was aligned in 12 mg/ml Pf1 phages yielding a D_2O splitting of 2.16 Hz. RDCs were measured using BEST-type HNCO and HN(CO)CA experiments (Rasia et al., 2011). ^{15}N relaxation dispersion was carried out at Nup153FG^{PxFG}/Importinβ concentrations of 250 μM and 180 μM, respectively, applying CPMG frequencies between 25 and 1,000 Hz (Schneider et al., 2015). All experiments were performed in Na-phosphate buffer (pH 6), 150 mM NaCl, 2 mM DTT, 5 mM $MgCl_2$, at 25°C and at a ^1H frequency of 600 MHz if not noted otherwise.

The conformational space available to disordered Nup153FG^{PxFG} was sampled using the *Flexible-meccano* statistical coil description (Ozenne et al., 2012) and representative ensembles in agreement with experimental chemical shifts were selected using ASTEROIDS (Jensen et al., 2010) and the ensemble was subsequently cross-validated against experimental RDCs and SAXS.

SmFRET Experiments

SmFRET measurements of dual labeled freely diffusing proteins were performed on a confocal geometry detecting donor and acceptor intensities (from which the FRET efficiency E_{FRET} is calculated) as well as fluorescence lifetimes (τ) on a custom built multiparameter setup as previously described (Milles and Lemke, 2011).

Fluorescence Stopped-Flow Experiments

The association kinetics were monitored by following the fluorescence anisotropy change of Nup153FG labeled at the indicated position with Cy3B (see sequences in Supplemental Experimental Procedures) upon binding to different concentrations of NTRs, under pseudo-first order conditions. Anisotropy (r) was calculated from fluorescence intensities measured with polarizing filters in the parallel (∥) and perpendicular (⊥) position.

Each trace was obtained by averaging ≥30 traces and background fluorescence was then subtracted. The anisotropy traces where fit with a biexponential function to determine k_{obs}. The different k_{obs} were plotted against the respective NTR concentrations and were linearly fit to obtain the association constant (k_{on}) from the slope.

The used BioLogic (Grenoble, France) stopped-flow equipment permits automatic titration and repeated technical replicates, which typically yield a small standard deviation. We derived an experimental error of ~20% in k_{on} measurements between different biological replicates. To be conservative, we thus do not show (the typically lower) standard deviations from technical replicates.

Transport Experiments

Routine reconstitution of the nucleocytoplasmic transport machinery in permeabilized cells was used and fluorescence cargo (NLS-MBP-eGFP) was imaged on a confocal microscope (Leica, Mannheim) at the indicated time points.

For single molecule tracking of NTRs, the same assay was used, but Importinβ-Alexa488 at single molecule concentration was tracked with an acquisition time of 2ms on a previously described home built imaging microscope (Ori et al., 2013).

All data analyses for FSF, FCS, smFRET and tracking were performed with custom written routines in IgorPro (Wavemetrics, OR).

MD and BD Simulations

The Nup153FG^{PxFG} fragment was modeled on the basis of its sequence that also included the exogenously inserted residues used for labeling of the fragment with fluorophores. For the binding simulations, Nup153FG^{PxFG} or Nup153^{FGFxFG} were randomly placed in a box of dimensions 15 × 15 × 15 nm^3 together with the N-terminal segment of Importinβ^N (PDB: 1F59). Brownian Dynamics (BD) simulations were performed starting from the MD complex that showed a specific association between the partners, and resembled the crystallographic binding pose as reported by ref. (Bayliss et al., 2000).

ACCESSION NUMBERS

The accession number for the data reported in this paper is Protein Ensemble Database (PED): 2AAE.

SUPPLEMENTAL INFORMATION

Supplemental Information includes Supplemental Experimental Procedures, seven figures, two tables, and three movies and can be found with this article online at http://dx.doi.org/10.1016/j.cell.2015.09.047.

AUTHOR CONTRIBUTIONS

S.M., D.M., I.V.A., designed and performed experiments, analyzed data and co-wrote the manuscript. M.R.J., N.B., C.K., S.T., J.C. provided additional reagents and analysis tools. S.L.S. designed experiments and analysis methods and co-wrote the manuscript. M.B., F.G. and E.A.L. conceived the project and co-wrote the manuscript.

ACKNOWLEDGMENTS

We are grateful for helpful comments and various discussions with Cedric Debes, Martin Beck as well as the whole Lemke group. We thank Guillaume Bouvignies for help with relaxation dispersion experiments, and Damien Maurin for sample preparation. S.M. acknowledges funding from the Boehringer Ingelheim Fonds (BIF) and an EMBO long-term fellowship (ALTF 468-2014) and EC (EMBOCOFUND2012, GA-2012-600394) via Marie Curie Action. I.V.A. acknowledges a BIF short-term fellowship. J.C. and S.L.S. are supported by the Wellcome Trust. J.C. is a Wellcome Trust Senior Research Fellow (WT/095195). E.A.L. is grateful to funds from the SFB1129 and the Emmy Noether program of the DFG, F.G. from the Klaus Tschira Foundation, and D.M. from the BIOMS program of Heidelberg University. We are also grateful to instrument access via the EMBL Pepcore facility.

Received: June 25, 2015
Revised: August 17, 2015
Accepted: September 23, 2015
Published: October 8, 2015

REFERENCES

Adams, R.L., and Wente, S.R. (2013). Uncovering nuclear pore complexity with innovation. Cell *152*, 1218–1221.

Arai, M., Ferreon, J.C., and Wright, P.E. (2012). Quantitative analysis of multi-site protein-ligand interactions by NMR: binding of intrinsically disordered p53 transactivation subdomains with the TAZ2 domain of CBP. J. Am. Chem. Soc. *134*, 3792–3803.

Bayliss, R., Littlewood, T., and Stewart, M. (2000). Structural basis for the interaction between FxFG nucleoporin repeats and importin-beta in nuclear trafficking. Cell *102*, 99–108.

Bednenko, J., Cingolani, G., and Gerace, L. (2003). Importin beta contains a COOH-terminal nucleoporin binding region important for nuclear transport. J. Cell Biol. *162*, 391–401.

Ben-Efraim, I., and Gerace, L. (2001). Gradient of increasing affinity of importin beta for nucleoporins along the pathway of nuclear import. J. Cell Biol. *152*, 411–417.

Brabez, N., Lynch, R.M., Xu, L., Gillies, R.J., Chassaing, G., Lavielle, S., and Hruby, V.J. (2011). Design, synthesis, and biological studies of efficient multivalent melanotropin ligands: tools toward melanoma diagnosis and treatment. J. Med. Chem. *54*, 7375–7384.

Bui, K.H., von Appen, A., DiGuilio, A.L., Ori, A., Sparks, L., Mackmull, M.T., Bock, T., Hagen, W., Andrés-Pons, A., Glavy, J.S., and Beck, M. (2013). Integrated structural analysis of the human nuclear pore complex scaffold. Cell *155*, 1233–1243.

Chekulaeva, M., Parker, R., and Filipowicz, W. (2010). The GW/WG repeats of Drosophila GW182 function as effector motifs for miRNA-mediated repression. Nucleic Acids Res. *38*, 6673–6683.

Cook, A., Bono, F., Jinek, M., and Conti, E. (2007). Structural biology of nucleocytoplasmic transport. Annu. Rev. Biochem. *76*, 647–671.

Csermely, P., Palotai, R., and Nussinov, R. (2010). Induced fit, conformational selection and independent dynamic segments: an extended view of binding events. Trends Biochem. Sci. *35*, 539–546.

Denning, D.P., Patel, S.S., Uversky, V., Fink, A.L., and Rexach, M. (2003). Disorder in the nuclear pore complex: the FG repeat regions of nucleoporins are natively unfolded. Proc. Natl. Acad. Sci. USA *100*, 2450–2455.

Dinkel, H., Van Roey, K., Michael, S., Davey, N.E., Weatheritt, R.J., Born, D., Speck, T., Krüger, D., Grebnev, G., Kuban, M., et al. (2014). The eukaryotic linear motif resource ELM: 10 years and counting. Nucleic Acids Res. *42*, D259–D266.

Dyson, H.J., and Wright, P.E. (2005). Intrinsically unstructured proteins and their functions. Nat. Rev. Mol. Cell Biol. *6*, 197–208.

Eisele, N.B., Labokha, A.A., Frey, S., Görlich, D., and Richter, R.P. (2013). Cohesiveness tunes assembly and morphology of FG nucleoporin domain meshworks - Implications for nuclear pore permeability. Biophys. J. *105*, 1860–1870.

Frey, S., and Görlich, D. (2007). A saturated FG-repeat hydrogel can reproduce the permeability properties of nuclear pore complexes. Cell *130*, 512–523.

Ganguly, D., Zhang, W., and Chen, J. (2013). Electrostatically accelerated encounter and folding for facile recognition of intrinsically disordered proteins. PLoS Comput. Biol. *9*, e1003363.

Hoelz, A., Debler, E.W., and Blobel, G. (2011). The structure of the nuclear pore complex. Annu. Rev. Biochem. *80*, 613–643.

Hough, L.E., Dutta, K., Sparks, S., Temel, D.B., Kamal, A., Tetenbaum-Novatt, J., Rout, M.P., and Cowburn, D. (2015). The molecular mechanism of nuclear transport revealed by atomic scale measurements. eLife *4*, 4.

Isgro, T.A., and Schulten, K. (2005). Binding dynamics of isolated nucleoporin repeat regions to importin-beta. Structure *13*, 1869–1879.

Jensen, M.R., Salmon, L., Nodet, G., and Blackledge, M. (2010). Defining conformational ensembles of intrinsically disordered and partially folded proteins directly from chemical shifts. J. Am. Chem. Soc. *132*, 1270–1272.

Jovanovic-Talisman, T., Tetenbaum-Novatt, J., McKenney, A.S., Zilman, A., Peters, R., Rout, M.P., and Chait, B.T. (2009). Artificial nanopores that mimic the transport selectivity of the nuclear pore complex. Nature *457*, 1023–1027.

Kalinin, S., Valeri, A., Antonik, M., Felekyan, S., and Seidel, C.A. (2010). Detection of structural dynamics by FRET: a photon distribution and fluorescence lifetime analysis of systems with multiple states. J. Phys. Chem. B *114*, 7983–7995.

Kragelj, J., Palencia, A., Nanao, M.H., Maurin, D., Bouvignies, G., Blackledge, M., and Jensen, M.R. (2015). Structure and dynamics of the MKK7-JNK signaling complex. Proc. Natl. Acad. Sci. USA *112*, 3409–3414.

Kramer, R.H., and Karpen, J.W. (1998). Spanning binding sites on allosteric proteins with polymer-linked ligand dimers. Nature *395*, 710–713.

Kubitscheck, U., Grünwald, D., Hoekstra, A., Rohleder, D., Kues, T., Siebrasse, J.P., and Peters, R. (2005). Nuclear transport of single molecules: dwell times at the nuclear pore complex. J. Cell Biol. *168*, 233–243.

Lim, R.Y., Fahrenkrog, B., Köser, J., Schwarz-Herion, K., Deng, J., and Aebi, U. (2007). Nanomechanical basis of selective gating by the nuclear pore complex. Science *318*, 640–643.

Lowe, A.R., Tang, J.H., Yassif, J., Graf, M., Huang, W.Y., Groves, J.T., Weis, K., and Liphardt, J.T. (2015). Importin-β modulates the permeability of the nuclear pore complex in a Ran-dependent manner. eLife *4*, 4.

Mercadante, D., Milles, S., Fuertes, G., Svergun, D.I., Lemke, E.A., and Gräter, F. (2015). Kirkwood-Buff Approach Rescues Overcollapse of a Disordered Protein in Canonical Protein Force Fields. J. Phys. Chem. B *119*, 7975–7984.

Milles, S., and Lemke, E.A. (2011). Single molecule study of the intrinsically disordered FG-repeat nucleoporin 153. Biophys. J. *101*, 1710–1719.

Milles, S., and Lemke, E.A. (2014). Mapping multivalency and differential affinities within large intrinsically disordered protein complexes with segmental motion analysis. Angew. Chem. Int. Ed. Engl. *53*, 7364–7367.

Morrison, J., Yang, J.C., Stewart, M., and Neuhaus, D. (2003). Solution NMR study of the interaction between NTF2 and nucleoporin FxFG repeats. J. Mol. Biol. *333*, 587–603.

Moussavi-Baygi, R., Jamali, Y., Karimi, R., and Mofrad, M.R. (2011). Brownian dynamics simulation of nucleocytoplasmic transport: a coarse-grained model for the functional state of the nuclear pore complex. PLoS Comput. Biol. *7*, e1002049.

Ori, A., Banterle, N., Iskar, M., Andrés-Pons, A., Escher, C., Khanh Bui, H., Sparks, L., Solis-Mezarino, V., Rinner, O., Bork, P., et al. (2013). Cell type-specific nuclear pores: a case in point for context-dependent stoichiometry of molecular machines. Mol. Syst. Biol. *9*, 648.

Otsuka, S., Iwasaka, S., Yoneda, Y., Takeyasu, K., and Yoshimura, S.H. (2008). Individual binding pockets of importin-beta for FG-nucleoporins have different binding properties and different sensitivities to RanGTP. Proc. Natl. Acad. Sci. USA *105*, 16101–16106.

Ozenne, V., Bauer, F., Salmon, L., Huang, J.R., Jensen, M.R., Segard, S., Bernadó, P., Charavay, C., and Blackledge, M. (2012). Flexible-meccano: a tool for the generation of explicit ensemble descriptions of intrinsically disordered proteins and their associated experimental observables. Bioinformatics *28*, 1463–1470.

Peters, R. (2009). Translocation through the nuclear pore: Kaps pave the way. BioEssays *31*, 466–477.

Rasia, R.M., Lescop, E., Palatnik, J.F., Boisbouvier, J., and Brutscher, B. (2011). Rapid measurement of residual dipolar couplings for fast fold elucidation of proteins. J. Biomol. NMR *51*, 369–378.

Schleicher, K.D., Dettmer, S.L., Kapinos, L.E., Pagliara, S., Keyser, U.F., Jeney, S., and Lim, R.Y. (2014). Selective transport control on molecular velcro made from intrinsically disordered proteins. Nat. Nanotechnol. *9*, 525–530.

Schneider, R., Maurin, D., Communie, G., Kragelj, J., Hansen, D.F., Ruigrok, R.W., Jensen, M.R., and Blackledge, M. (2015). Visualizing the molecular recognition trajectory of an intrinsically disordered protein using multinuclear relaxation dispersion NMR. J. Am. Chem. Soc. *137*, 1220–1229.

Schoch, R.L., Kapinos, L.E., and Lim, R.Y. (2012). Nuclear transport receptor binding avidity triggers a self-healing collapse transition in FG-nucleoporin molecular brushes. Proc. Natl. Acad. Sci. USA *109*, 16911–16916.

Schuler, B., and Eaton, W.A. (2008). Protein folding studied by single-molecule FRET. Curr. Opin. Struct. Biol. *18*, 16–26.

Shammas, S.L., Travis, A.J., and Clarke, J. (2013). Remarkably fast coupled folding and binding of the intrinsically disordered transactivation domain of cMyb to CBP KIX. J. Phys. Chem. B *117*, 13346–13356.

Shammas, S.L., Travis, A.J., and Clarke, J. (2014). Allostery within a transcription coactivator is predominantly mediated through dissociation rate constants. Proc. Natl. Acad. Sci. USA *111*, 12055–12060.

Shoemaker, B.A., Portman, J.J., and Wolynes, P.G. (2000). Speeding molecular recognition by using the folding funnel: the fly-casting mechanism. Proc. Natl. Acad. Sci. USA *97*, 8868–8873.

Solyom, Z., Schwarten, M., Geist, L., Konrat, R., Willbold, D., and Brutscher, B. (2013). BEST-TROSY experiments for time-efficient sequential resonance assignment of large disordered proteins. J. Biomol. NMR *55*, 311–321.

Spaar, A., Dammer, C., Gabdoulline, R.R., Wade, R.C., and Helms, V. (2006). Diffusional encounter of barnase and barstar. Biophys. J. *90*, 1913–1924.

Tetenbaum-Novatt, J., Hough, L.E., Mironska, R., McKenney, A.S., and Rout, M.P. (2012). Nucleocytoplasmic transport: a role for nonspecific competition in karyopherin-nucleoporin interactions. Mol. Cell. Proteomics *11*, 31–46.

Tompa, P., and Fuxreiter, M. (2008). Fuzzy complexes: polymorphism and structural disorder in protein-protein interactions. Trends Biochem. Sci. *33*, 2–8.

Toretsky, J.A., and Wright, P.E. (2014). Assemblages: functional units formed by cellular phase separation. J. Cell Biol. *206*, 579–588.

Tu, L.C., Fu, G., Zilman, A., and Musser, S.M. (2013). Large cargo transport by nuclear pores: implications for the spatial organization of FG-nucleoporins. EMBO J. *32*, 3220–3230.

Wagner, R.S., Kapinos, L.E., Marshall, N.J., Stewart, M., and Lim, R.Y. (2015). Promiscuous binding of Karyopherinβ1 modulates FG nucleoporin barrier function and expedites NTF2 transport kinetics. Biophys. J. *108*, 918–927.

Wälde, S., and Kehlenbach, R.H. (2010). The Part and the Whole: functions of nucleoporins in nucleocytoplasmic transport. Trends Cell Biol. *20*, 461–469.

Wright, P.E., and Dyson, H.J. (2009). Linking folding and binding. Curr. Opin. Struct. Biol. *19*, 31–38.

Yamada, J., Phillips, J.L., Patel, S., Goldfien, G., Calestagne-Morelli, A., Huang, H., Reza, R., Acheson, J., Krishnan, V.V., Newsam, S., et al. (2010). A bimodal distribution of two distinct categories of intrinsically disordered structures with separate functions in FG nucleoporins. Mol. Cell. Proteomics *9*, 2205–2224.

Ziarek, J.J., Veldkamp, C.T., Zhang, F., Murray, N.J., Kartz, G.A., Liang, X., Su, J., Baker, J.E., Linhardt, R.J., and Volkman, B.F. (2013). Heparin oligosaccharides inhibit chemokine (CXC motif) ligand 12 (CXCL12) cardioprotection by binding orthogonal to the dimerization interface, promoting oligomerization, and competing with the chemokine (CXC motif) receptor 4 (CXCR4) N terminus. J. Biol. Chem. *288*, 737–746.